Radiation due to CO_2 or H_2O and Particles in Cylindrical Media

S. T. Thynell*
The Pennsylvania State University, University Park, Pennsylvania 16802

This study considers nongray, absorbing, emitting, anisotropically scattering, one-dimensional, radiative transfer in cylindrical media. The radiation transfer is due to a gas composed of either CO_2 or H_2O, soot and particles. The temperature of these constituents is equal and uniform throughout the medium. The nongray effects are due to the spectrally discontinuous absorption/emission behavior of the gas and the spectrally continuous absorption/emission behavior of the soot. The absorption coefficient of the nongray gas is modeled according to Edwards' exponential wide-band models. The absorption coefficient of the soot is inversely proportional to wavelength. The scattering phase function of the gray particles is represented as the sum of an isotropic component and a delta-function. An accurate solution to this problem is obtained by using the P_1-approximation coupled with the integral form of the equation of transfer. The bandwidths are determined by utilizing the wide-band models, and the spectral integration is performed over all wavelengths according to a two-point quadrature for each band. Comprehensive parameter surveys are performed in order to establish a detailed understanding of the complex interaction between radiatively participating particles and molecular gases.

Nomenclature

A_ν = constant in P_1-approximation
a_i = 1 for an asymmetric band
= 2 for a symmetric band
C = correction factor
C_s = constant in Eq. (7) for soot absorption coefficient
f = scattering factor, Eq. (8)
f_v = soot volume fraction
$G_\nu(r)$ = spectral incident radiation
$I_{b\nu}(T)$ = Planck blackbody function
$I_n(x)$ = nth order modified Bessel function of the first kind
$I_\nu(r,\theta,\phi)$ = spectral radiation intensity
$I_\nu^{\pm}(r,\theta,\phi)$ = forward and backward radiation intensities
L = length
M = order of quadrature
N = number of gas absorption bands
$P(\Theta)$ = scattering phase function
p = pressure
$q_\nu^r(r)$ = spectral net radiative heat flux
$q_{\nu,sp}^r(r)$ = spectral net radiative heat flux due to soot and particles
R_{ph} = physical or geometric radius
R_ν = spectral optical radius at $r_{ph} = R_{ph}$
r_{ph} = physical or geometric radial coordinate
$r_{s\nu}$ = scaled spectral optical radius, Eq. (9a)
r_ν = spectral optical radius
(S/d) = mean line intensity to spacing ratio
T = temperature
$T_1(r,\xi_\nu)$ = integral defined in Ref. 15
$U_1(r)$ = integral defined in Ref. 15
$W(\xi_\nu)$ = integral defined in Ref. 15
w_k = quadrature point in Mth order integration
$Y_1(r)$ = integral defined in Ref. 15
α_i = integrated band intensity
β_ν = extinction coefficient
ϵ = emissivity
ϵ_{max} = spectral emissivity at band head
η = pressure broadening parameter
θ = polar angle
Θ = scattering angle
κ = absorption coefficient
λ = wavelength
ν = wavenumber
$\nu_{i,j}$ = jth quadrature point of ith band
ν_{li} = lower limit wavenumber of ith band
ν_{ui} = upper limit wavenumber of ith band
ξ = eigenvalue
ρ_g = density of gas
σ_p = scattering coefficient
τ_L = optical depth at band head
τ_p = optical radius due to gray particles, Eq. (25)
ϕ = azimuth angle
ω_p = single scattering albedo due to particles, Eq. (24b)
ω_{ps} = scaled single scattering albedo due to particles, Eq. (24a)
$\omega_{p\nu}$ = single scattering albedo
$\omega_{s\nu}$ = scaled single scattering albedo, Eq. (9b)
$\bar{\omega}$ = exponential decay width
$\Delta\nu_i$ = width of ith band
$\Phi_1(r)$ = integral defined in Ref. 15

Subscripts
ci = band center of ith band
g = gas
H = hemispherical
i = ith band
p = particle
s = scaled
sp = soot and/or particles
w = wall surface
ν = spectral quantity

Received Dec. 9, 1988; revision received April 5, 1989; presented as Paper 89-1718 at the AIAA 24th Thermophysics Conference, Buffalo, NY, June 12-15, 1989.

*Assistant Professor, Department of Mechanical Engineering. Member AIAA.

Introduction

RADIATIVE heat transfer in cylindrical geometry is of considerable interest in many applications. Examples of such applications include, among others, the development of methods for improving the efficiency of furnaces, the analysis of heat transfer in stacks, the design of rocket engines, infrared (IR) signature studies of rocket plumes, and radiative transfer in stellar atmospheres. Radiation transfer in these situations is often coupled to conduction, convection, and chemical reactions in a highly nonlinear manner. Consequently, such problems are usually solved iteratively by numerical methods, which may be very time consuming on the computer. In order to reduce such computational times, it is of considerable importance to have efficient and simple yet accurate radiation models.

The analysis of radiation in cylindrical geometry has been the subject of numerous investigations. Felske and Lee[1] analyzed radiation in an absorbing/emitting, isothermal cylinder containing particulate whose absorption coefficient was inversely proportional to wavelength and whose walls were black. Subsequently, Tabanfar and Modest[2] extended the analysis to include the effects of nongray gases. Radiative transfer due to gray absorbing/emitting, scattering particles confined in a one-dimensional cylinder has been studied by various workers. Azad and Modest[3] employed a numerical integration method for solving the corresponding integral form of the equation of transfer including the effects of linear anisotropic scattering. Recently, Der and Nelson[4] used a Monte Carlo scheme to compute the emissivity of a cylindrical medium containing alumina particles.

There are several works available in the literature that have analyzed the effects of gray, isotropically scattering particles and nongray gases in plane-parallel media. Buckius and Fernandez-Fraga[5] demonstrated the use of the optical path length approach for obtaining an approximate solution to the equation of transfer. Buckius[6] subsequently applied this approach for studying the reflection, transmission, and emission from an isothermal, plane-parallel medium. To show the effects of real gases, Skocypec and Buckius[7] presented results for the normal emittance of an isothermal plane layer containing gray, isotropically scattering particles and either H_2O or CO_2.

It appears, however, that studies having the objective of analyzing the effects of a nongray gas, soot, and scattering particles on the radiative transfer in a one-dimensional cylinder are not available in the literature in spite of the numerous areas of application of such works. There are two objectives of the present work: 1) to formulate and present a simple yet accurate solution method for an isothermal medium containing nongray, absorbing, emitting, anisotropically scattering constituents and 2) to assess the effects of nongray gases, soot, and scattering particles on the total hemispherical emissivity. A rigorous and systematic assessment of the roles of these constituents should provide a guide to reducing the complexity of models of interaction problems while maintaining sufficient accuracy and therefore should save important computer time.

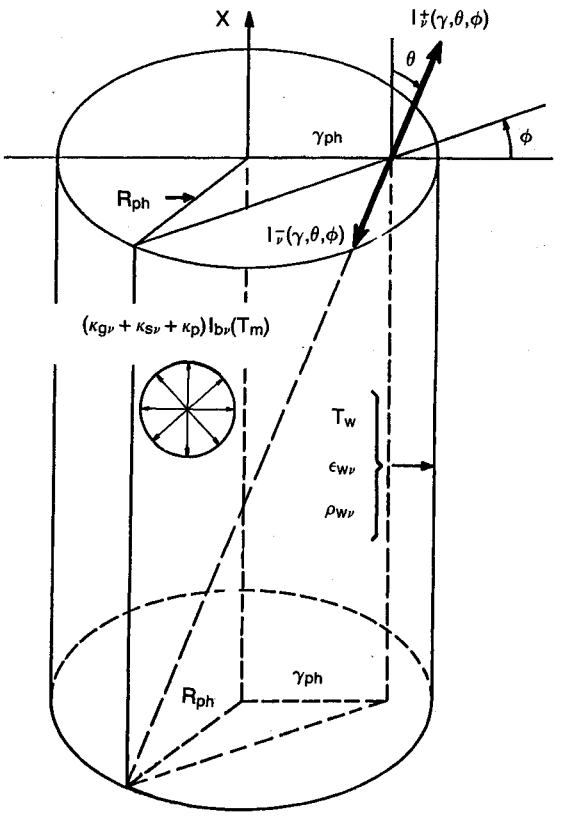

Fig. 1 Physical model and coordinates.

Analysis

Equation of Radiative Transfer

Radiative transfer is considered in an absorbing, emitting, anisotropically scattering cylindrical medium occupying the region $0 \le r \le R$, in which a molecular gas, soot, and particles participate in the radiative heat exchange. In this work, we define "soot" as very small particles that only absorb radiation and "particles" as much larger particles that both absorb and scatter the radiation. It is assumed that the temperature as well as the concentration of the gas/soot/particle mixture is uniform in directions along and around the x axis, as shown in Fig. 1. Hence the scattering and extinction coefficients are independent of position. The spectral equation of transfer is given by[8]

$$\left[\sin\theta\cos\phi\frac{\partial}{\partial r_\nu}-\sin\theta\frac{\sin\phi}{r_\nu}\frac{\partial}{\partial\phi}+1\right]I_\nu(r_\nu,\theta,\phi)$$

$$=(1-\omega_{p\nu})I_{b\nu}(T_m)+\frac{\omega_{p\nu}}{4\pi}\int_{\phi'=0}^{2\pi}\int_{\theta'=0}^{\pi}$$

$$\times I_\nu(r_\nu,\theta',\phi')P(\cos\Theta)\sin\theta'\,d\theta'\,d\phi'$$

$$0<r_\nu<R_\nu,\ 0\le\theta\le\pi,\quad 0\le\phi\le 2\pi \qquad (1)$$

Assuming that the opaque bounding surface is at a prescribed temperature T_w and reflects incident radiation diffusely, the corresponding boundary condition is of the form

$$I_\nu^-(R_\nu,\theta,-\phi)=\epsilon_{w\nu}I_{b\nu}(T_w)+\frac{4(1-\epsilon_{w\nu})}{\pi}$$

$$\times\int_{\phi'=0}^{\frac{\pi}{2}}\int_{\theta'=0}^{\frac{\pi}{2}}I_\nu^+(R_\nu,\theta',\phi')\cos\phi'\sin^2\theta'\,d\theta'\,d\phi'$$

$$0\le\theta\le\pi,\ -\frac{\pi}{2}\le\phi\le\frac{\pi}{2} \qquad (2)$$

The single scattering albedo $\omega_{p\nu}$ is the ratio of the scattering coefficient σ_p and the extinction coefficient β_ν, i.e., $\omega_{p\nu}=\sigma_p/\beta_\nu$, where the spectral extinction coefficient β_ν accounts for the attenuation of radiation by the gas, soot, and particles confined inside the cylinder. It is assumed that the absorption coefficients of the gas and soot are spectrally dependent and written as $\kappa_{g\nu}$ and $\kappa_{s\nu}$, respectively; whereas the absorption and scattering coefficients of the particles are spectrally independent and written as κ_p and σ_p, respectively. The extinction coefficient and spectral optical radius r_ν, respectively, become

$$\beta_\nu=\kappa_{g\nu}+\kappa_{s\nu}+\kappa_p+\sigma_p \qquad (3a)$$

and

$$r_\nu = \beta_\nu r_{ph} \tag{3b}$$

where r_{ph} is the physical radial coordinate of the medium.

Gaseous Absorption Coefficient

To obtain an approximate expression for the gaseous absorption coefficient, valid in spectral regions ranging from the weak to the strong line limits, the Goody model is employed in the following manner. First, assuming that Kirchhoff's law is applicable, the spectral gas emissivity is written as[9]

$$\epsilon_{g\nu} = 1 - \exp\left[-\frac{(S/d)\rho_g L}{[1 + (S/d)\rho_g L/\eta]^{1/2}} \right] \tag{4}$$

where (S/d) is the mean line intensity to spacing ratio, ρ_g the density of the absorbing species, L the length, and η is the mean line width to spacing parameter. For values of $\eta \geq 1$, which often is the case for gases at high pressures, there is significant overlapping of the spectral lines, and the spectral emissivity is well approximated by simply letting $\eta \to \infty$ in Eq. (4).[10] Such approximation yields good results for CO_2 but less accurate results for H_2O, whose line structure is much more pressure sensitive. To obtain a "best" fit of the band shapes, $(S/d)_i$ of the ith band is approximated according to the exponential-tailed, wide-band model[9] as

$$(S/d)_i = \frac{\alpha_i}{\bar{\omega}_i} \exp(-a_i|\nu - \nu_{ci}|/\bar{\omega}_i) \tag{5}$$

where α_i is the integrated band intensity, $\bar{\omega}_i$ the exponential decay width, ν_{ci} the location of band center, $a_i = 1$ for an asymmetric band and $a_i = 2$ for a symmetric band. It is now assumed that the terms within the argument of the exponential in Eq. (4) are equivalent to a product of the gaseous absorption coefficient and a length. Such assumption yields an *approximate* expression for the gaseous absorption coefficient given by

$$\kappa_{g\nu_i} = \frac{(S/d)_i \rho_g}{[1 + (S/d)_i \rho_g L_{mb}/\eta_i]^{1/2}} \tag{6}$$

where L has been replaced by the mean beam length L_{mb}, which in cylindrical geometry is approximately given by $L_{mb} = 1.9R_{ph}$.[9] Thus, the gaseous absorption coefficient, which is a function of temperature, density, and mean beam length (or pressure path length), in the high pressure limit reduces to the same expression used by other workers.[6,7,9]

Soot Absorption Coefficient

The absorption coefficient of the soot is spectrally continuous and accurately represented by the expression[11]

$$\kappa_{s\nu} = C_s/\lambda^n \tag{7}$$

where $C_s = c_0 f_v$ with f_v being the soot volume fraction and c_0 a constant whose value is between 3 and 7. Although the value of the exponent n is approximately equal to unity, which is assumed in this work, it depends weakly on wavelength and on the type of fuel being represented.[11]

Scattering Phase Function

For highly forward scattering particle suspensions, the Dirac-delta scattering phase function is both a reasonably accurate and convenient description of the actual scattering phase function. Therefore, the Dirac-delta scattering phase function is incorporated into the present formulation and written as[12]

$$P(\cos\Theta) = 1 - f + 4\pi f \delta(\cos\theta - \cos\theta')\delta(\phi - \phi') \tag{8}$$

where the factor $f = 0$ indicates isotropic scattering and $0 < f \leq 1$ forward scattering. By introducing Eq. (8) into Eq. (1) and performing some rearrangement, one obtains an equation of transfer for an isotropically scattering medium with a spectrally scaled optical radius and single scattering albedo given by

$$r_{s\nu} = (1 - \omega_{p\nu} f) r_\nu \tag{9a}$$

and

$$\omega_{s\nu} = \frac{\omega_{p\nu}(1 - f)}{(1 - f\omega_{p\nu})} \tag{9b}$$

That is, the optical radius r_ν and single scattering albedo $\omega_{p\nu}$ in Eq. (1) are replaced by the scaled quantities $r_{s\nu}$ and $\omega_{s\nu}$, respectively, and the scattering phase function $P(\cos\Theta) = 1$. In addition, to maintain a reasonable level of clarity in the subsequent analysis, the subscripts s and wavenumber ν are omitted on the scaled spectral optical radius.

Spectral Solution to Equation of Transfer

To obtain a solution to the previously described problem, the well-known P_1-approximation is first used. By following the analysis of Kofink,[13] it is easily shown that the solution to the radiation problem using the P_1-approximation based on a Marshak condition[8] is

$$G_\nu(r) = A_\nu I_0(r/\xi_\nu) + 4\pi I_{b\nu}(T_m) \tag{10}$$

where $G_\nu(r)$ is the incident radiation, which is defined by

$$G_\nu(r) = \int_{\phi=0}^{2\pi} \int_{\theta=0}^{\pi} I_\nu(r,\theta,\phi) \sin\theta \, d\theta \, d\phi \tag{11}$$

Furthermore, $I_n(x)$ are the modified Bessel functions, the eigenvalue ξ_ν is computed from

$$\xi_\nu = 1/[3(1 - \omega_{s\nu})]^{1/2} \tag{12}$$

and the constant A_ν is given by

$$A_\nu = \frac{4\pi\epsilon_{w\nu}[I_{b\nu}(T_w) - I_{b\nu}(T_m)]}{\epsilon_{w\nu} I_0(R/\xi_\nu) + \frac{2}{3\xi_\nu}(2 - \epsilon_{w\nu}) I_1(R/\xi_\nu)} \tag{13}$$

Since the P_1-approximation in some cases may give physically unrealistic results,[8] it is desirable to improve the solution to radiative heat transfer. In this work, however, we are primarily interested in the net radiative heat flux $q_\nu^r(r)$, which is defined by

$$q_\nu^r(r) = \int_{\phi=0}^{2\pi} \int_{\theta=0}^{\pi} I_\nu(r,\theta,\phi) \cos\phi \sin^2\theta \, d\theta \, d\phi \tag{14}$$

To obtain the improvement in the solution, we employ the integral form of the scaled version of the equation of transfer. Using the recently developed results,[14] it may be shown that by substituting Eq. (10) into the integral form of the equation of transfer that the improved solution for the net radiative heat flux is given by

$$q_\nu^r(r) = -Y_1(r) + \frac{\omega_{s\nu}}{4\pi} A_\nu [T_1(r,\xi_\nu) - (1 - \epsilon_{w\nu}) E U_1(r) W(\xi_\nu)] + I_{b\nu}(T_m)[\Phi_1(r) - (1 - \epsilon_{w\nu}) E U_1(r) U_1(R)] \tag{15}$$

where

$$Y_1(r) = \epsilon_{w\nu} \pi I_{b\nu}(T_w) E U_1(r) \tag{16a}$$

$$E = \frac{R}{\pi[\epsilon_{w\nu} + \frac{1}{\pi}(1 - \epsilon_{w\nu}) R U_1(R)]} \tag{16b}$$

and explicit expressions for the functions $U_1(r)$, $T_1(r,\xi_\nu)$, $W(\xi_\nu)$, and $\Phi_1(r)$ are available.[15]

Integration over All Wavenumbers $0 \le \nu \le \infty$

To analyze problems in which radiation interacts with other modes of energy transfer, it is necessary to add up the radiation contribution from all wavenumbers. Consequently, an integration of Eq. (15) over the complete wavenumber spectrum must be performed. To perform such integration in a simple yet accurate manner, a two-point Gauss-Legendre formula for each band will be employed. The integration is complicated by the fact that some bands may overlap, and the treatment of such effects are discussed in the Appendix. To perform the integration over each band, the bandwidths $\Delta\nu_i$, $i = 1, 2, \ldots, N$ are first determined.

To obtain the bandwidth, the spectral gas emissivity given by Eq. (4) will be utilized. First, the mean beam length will be approximated as $L_{mb} = 1.9R_{ph}$, where R_{ph} is the physical radius of the cylinder.[9] Second, it will be assumed that the wavenumber at which the spectral emissivity reduces to a fraction of its maximum, $\epsilon = b\epsilon_{\max}$, yields a definition for the bandwidth $\Delta\nu_i$. The use of Eqs. (4-6) in this manner leads to the following expression for the bandwidth:

$$\Delta\nu_i = -\bar{\omega}_i \, ln\left\{\frac{Z_i}{2\tau_{L,i}}\left[\frac{1}{\eta_i}+\sqrt{\frac{1}{\eta_i^2}+\frac{4}{Z_i}}\right]\right\} \tag{17}$$

where

$$\tau_{L,i} = \alpha_i \rho_g L_{mb}/\bar{\omega}_i \tag{18a}$$

$$Z_i = ln^2[(1-b\epsilon_{\max,i})^{-1}] \tag{18b}$$

$$\epsilon_{\max,i} = 1-\exp[-\tau_{L,i}/(1+\tau_{L,i}/\eta_i)^{1/2}] \tag{18c}$$

It should be noted that Eq. (17) is applicable for both symmetric and asymmetric bands; that is, $\Delta\nu_i = \nu_{ui} - \nu_{li}$ for a symmetric band, or $\Delta\nu_i = \nu_{ci} - \nu_{li}$ for an asymmetric band, such as the 4.3 μm CO_2 band. To further simplify the analysis, the following additional assumptions are introduced: 1) the blackbody function and the soot absorption coefficient does not vary appreciably over a gas absorption band and 2) they can be represented by their values at the band center. That is, only the spectral variation of the gaseous absorption coefficient is accounted for within a band. These assumptions yield symmetric bands, and, therefore, a reduction in the numerical integration effort is achieved (for the symmetric bands). However, these assumptions are not employed when performing the spectral integration for the water vapor rotational band as discussed in the Appendix. The zeros of the quadrature are now shifted from the interval $(-1, 1)$ to either the lower wavenumber interval (ν_{li}, ν_{ci}) or to the upper wavenumber interval (ν_{ci}, ν_{ui}). For example, the quadrature points shifted to the lower wavenumber interval are given by

$$\nu_{i,1} = \nu_{ci} - 0.2113\Delta\nu_i/a_i \tag{19a}$$

and

$$\nu_{i,2} = \nu_{ci} - 0.7887\Delta\nu_i/a_i \tag{19b}$$

The wavenumber integration must also account for the radiation contribution from soot and particles in between the bands; this contribution is denoted by $q_{\nu,sp}(r)$. However, it is not desirable to introduce another bandwidth that accounts for the soot/particle effects. Instead, a soot/particle radiation contribution over each band is added to the soot/particle contribution in between the bands and then subtracted from the already specified gas/soot/particle bands. This procedure results in the spectral integration over all wavenumbers given by

$$q^r(r_{ph}) = \sum_{i=1}^{N}\Delta\nu_i\left[\frac{1}{2}\sum_{j=1}^{2} q^r_{\nu_{ij}}(r) - q_{\nu_i,sp}(r)\right] + \int_0^\infty q_{\nu,\,sp}(r)\mathrm{d}\nu \tag{20}$$

when N is the number of gas absorption bands. The integration of the spectrally continuous soot/particle contribution may be approximated by an Mth order quadrature as

$$\int_0^\infty q_{\nu,\,sp}(r)\mathrm{d}\nu = \sum_{k=1}^{M} w_k q_{\nu_k,sp}(r) \tag{21}$$

where w_k, and ν_k, $k = 1, 2, \ldots, M$ are the weights and quadrature points, respectively. It should be noted that the functional dependence of q^r in Eq. (20) is written in terms of the physical radial coordinate r_{ph}. A 40-point Gauss-Legendre quadrature is employed in this work to approximate the integral in Eq. (21).

Discussion of Results

Accuracy of Solution

To illustrate the application of the previously described analysis and to limit the volume of results, we consider a medium bounded by a black cylindrical wall ($\epsilon_{w\nu} = 1$), which is maintained at $T_w \to 0$K. For this case, it is of interest to first check the accuracy of the solution for various scattering albedos and optical dimensions. For this purpose, results are presented of the spectral hemispherical emissivity ($\epsilon_{H\nu}$) computed by the P_1-approximation, the integral form given by Eq. (15) and the "exact" solution.[15] It is easily shown that the spectral hemispherical emissivity by the P_1-approximation and the improved solution according to Eq. (15) reduce to, respectively, the expressions given by

$$\epsilon_{H\nu} = (1-\omega_{s\nu})\frac{4\xi I_1(R/\xi)}{I_0(R/\xi)+\frac{2}{3\xi}I_1(R/\xi)} \tag{22a}$$

and

$$\epsilon_{H\nu} = \frac{1}{\pi}\left[RU_1(R) - \frac{\omega_{s\nu}T_1(R,\xi)}{I_0(R/\xi)+\frac{2}{3\xi}I_1(R/\xi)}\right] \tag{22b}$$

In Table 1, the accuracy of the solution methods is illustrated for the various scaled spectral optical radii $R = 0.1$, 1, and 10, and for the different spectral single scattering albedos, $\omega_{s\nu} = 0.01$, 0.1, 0.5, 0.9, and 0.99. Examination of this table reveals that the P_1-approximation overpredicts the emissivity by as much as 6% for small values of the single scattering albedos; for larger optical radii ($R > 10$), the emissivity is above unity, which is physically impossible. The improved solution, on the other hand, in all cases predicts physically realistic values although the maximum error compared to the exact solution is about 5%. In addition, the exact solution of the spectral hemispherical emissivity is obtained as the scattering albedo $\omega_{s\nu} \to 0$. Thus a substitution of the solution from the P_1-approximation into the integral form of the equation of transfer yields physically realistic results. The improved results should be of sufficient accuracy for most engineering applications.

Table 1 Numerical results of the spectral hemispherical emissivity ϵ_{H_ν} for a cylinder of spectral optical radius R and spectral single scattering albedo $\omega_{s\nu}$ bounded by a black wall at zero temperature obtained by using Eqs. (22a) and (22b) and an "exact" solution method

		Spectral hemispherical emissivity $\epsilon_{H\nu}$		
R	$\omega_{s\nu}$	Eq. (22a)	Eq. (22b)	Exact
0.1	0.01	0.1796	0.1754	0.1754
	0.10	0.1646	0.1608	0.1611
	0.50	0.0951	0.0929	0.0939
	0.90	0.0198	0.0193	0.0197
	0.99	0.0020	0.0020	0.0020
1.0	0.01	0.8526	0.8106	0.8108
	0.10	0.8163	0.7759	0.7773
	0.50	0.5964	0.5659	0.5734
	0.90	0.1759	0.1666	0.1736
	0.99	0.0197	0.0187	0.0197
10.0	0.01	1.0544	0.9957	0.9959
	0.10	1.0299	0.9732	0.9750
	0.50	0.8779	0.8340	0.8422
	0.90	0.4961	0.4804	0.4872
	0.99	0.1393	0.1376	0.1386

Table 2 Total hemispherical emissivity ϵ_{H,CO_2} for a cylinder containing CO_2 and a transparent gas of 1 atm total pressure with $p_{CO_2} \to 0$ bounded by a black wall a zero temperature

		Total hemispherical emissivity ϵ_{H,CO_2}		
T_g K	$p_{CO_2}L_{mb}$ atm-m	Present method	Hottel (1954)	Error %
833	0.0030	0.0286	0.0300	−5
	0.0091	0.0469	0.0500	−6
	0.0244	0.0669	0.0720	−7
	0.0609	0.0890	0.0960	−7
	0.1827	0.1205	0.1150	5
	0.6090	0.1618	0.1500	8
1111	0.0030	0.0249	0.0250	−1
	0.0091	0.0432	0.0470	−8
	0.0244	0.0634	0.0700	−9
	0.0609	0.0868	0.0930	−7
	0.1827	0.1220	0.1200	2
	0.6090	0.1683	0.1750	4
1389	0.0030	0.0187	0.0200	−6
	0.0091	0.0347	0.0380	−9
	0.0244	0.0529	0.0570	−7
	0.0609	0.0747	0.0800	−7
	0.1827	0.1094	0.1100	−1
	0.6090	0.1550	0.1500	4
1667	0.0030	0.0135	0.0135	0
	0.0091	0.0266	0.0280	−5
	0.0244	0.0421	0.0430	−2
	0.0609	0.0611	0.0630	−3
	0.1827	0.0927	0.0950	−2
	0.6090	0.1363	0.1300	5
1944	0.0030	0.0097	0.0105	−8
	0.0091	0.0201	0.0205	−2
	0.0244	0.0331	0.0340	−3
	0.0609	0.0492	0.0510	−4
	0.1827	0.0760	0.0780	−2
	0.6090	0.1162	0.1150	1

Total Hemispherical Emissivity of CO_2

To illustrate the accuracy of the two-point quadrature, the total hemispherical emissivity of CO_2 is compared by the present solution technique considering the 15, 10.4, 9.4, 4.3, 2.7, and 2.0 μm bands and compared to the experimental results of Hottel.[16] Such comparison is necessary in order to validate the calculational procedure, which is based on setting $b = 0.05$ in Eq. (18b) and adjusting the table value of the exponential decay widths $\bar{\omega}_i$ by 30%.[9] In Table 2, the total hemispherical emissivity of CO_2 in a mixture of nonradiating gases at 1 atm total pressure and results from Hottel[16] for the different gas temperatures $T_m = 833$, 1111, 1389, 1667, and 1944 K with pressure path lengths $p_{CO_2}L_{mb} = 0.003$, 0.0091, 0.0244, 0.0609, 0.1827, and 0.609 atm-m are shown. Inspection of Table 2 reveals an excellent agreement between the experimental and calculated values of the total hemispherical emissivity. In the worst case, the emissivity is underestimated by 9%. Such agreement between experimental and calculated values is rather surprising, since 1) the exponential wide-band model parameters are correlated to within 15% of the experimental data and 2) it is assumed that $L_{mb} = 1.9R_{ph}$, i.e., independent of the optical depth at the band head (τ_L). As discussed by Edwards,[9] the mean beam length in the high-pressure limit ($\eta \to \infty$) varies from $2R_{ph}$ for small optical depths ($\tau_L < 0.25$) to about $1.78R_{ph}$ for larger optical depths at the band head ($\tau_L > 5$).

Table 3 Total hemispherical emissivity ϵ_{H,H_2O} for a cylinder containing H_2O and a transparent gas of 1 atm total pressure with $p_{H_2O} \to 0$ bounded by a black wall at zero temperature

		Total hemispherical emissivity ϵ_{H,H_2O}			
T_g K	$p_{H_2O}L_{mb}$ atm-m	Present method	Hottel (1954)	Ludwig et al. (1973)	Edwards (1976)
500	0.010	0.0623	0.0490	0.0510	0.0570
	0.020	0.0886	0.0760	0.0740	0.0810
	0.100	0.1812	0.1800	0.1600	0.1700
	0.200	0.2362	0.2400	0.2000	0.2300
	2.000	0.4689	0.4800	0.4100	0.4300
1000	0.010	0.0348	0.0260	0.0330	0.0320
	0.020	0.0539	0.0450	0.0530	0.0500
	0.100	0.1307	0.1300	0.1300	0.1300
	0.200	0.1785	0.1800	0.1800	0.1800
	2.000	0.4022	0.4300	0.4200	0.4100
1500	0.010	0.0201	0.0130	0.0200	0.0180
	0.020	0.0335	0.0240	0.0330	0.0330
	0.100	0.0946	0.0850	0.1050	0.1100
	0.200	0.1373	0.1300	0.1600	0.1600
	2.000	0.3475	0.3300	0.4200	0.3800
2000	0.010	0.0114	0.0065	0.0110	0.0090
	0.020	0.0198	0.0130	0.0200	0.0180
	0.100	0.0648	0.0460	0.0770	0.0760
	0.200	0.1004	0.0880	0.1200	0.1200
	2.000	0.2916	0.2300	0.4000	0.3300

Total Hemispherical Emissivity of H_2O

In Table 3, the results of the total hemispherical emissivity ϵ_{H,H_2O} for a cylinder containing gaseous water vapor in an otherwise transparent gas at 1 atm total pressure in the limit as the partial pressure $p_{H_2O} \to 0$ are shown. These calculations have been based on including the five important bands of H_2O: the pure rotational band, which band model parameters have been updated to include the improvements suggested by Modak[17] and the vibrational-rotational bands having band centers located at 6.3, 2.7, 1.87, and 1.38 μm. The calculations are based on setting $b = 0.05$ in Eq. (18b) and adjusting the exponential decay width $\bar{\omega}_i$ for the vibration-rotation bands by 30%.[9] Inspection of Table 3 reveals an excellent agreement between the calculated results from the method outlined in this work, the experimental results of Hottel,[16] and the theoretical results of Ludwig et al.[18] and Edwards.[9]

Total Hemispherical Emissivity of Gas, Soot, and Particles

The total hemispherical emissivity for a medium containing gases, soot, and particles depends on several parameters including, among others, the pressure path length, soot volume fraction distance (C_sR_{ph}), mixture temperature, scaled optical radius, and scaled single scattering albedo. To deduce cases for which the gaseous radiation is of importance, it is convenient

to introduce an interaction parameter C defined as[7]

$$\epsilon_H = \epsilon_{H,\,sp} + C\epsilon_{H,\,g} \tag{23}$$

Such definition leads to the interpretation that for $C>1$, the particulate phase enhances the gas emissivity; for $C=1$, the particulate phase is transparent to the gaseous emission; and for $C<1$, the particulate phase shields the gaseous emission. If $0\le C\le 1$, then one may interpret the interaction parameter as an effective transmissivity of the particular matter. However, in the corresponding case of plane-parallel geometry, a thorough search through the parameter space has revealed that the interaction parameter $C\le 1.03$.[19] That is, the presence of scattering particles within the medium almost always reduces the emissivity. It is clear that a similar parameter could be defined for the interaction between *soot* and *particles*, but to limit the volume of results, such parameter is not introduced in this work. However, to use Eq. (23), it is necessary that $\epsilon_{H,\,sp}$ is known; therefore such results are presented next.

In Figs. 2-6 the total hemispherical emissivity of a mixture containing soot and particles for temperatures ranging from 500 to 2000 K, soot volume fraction distances $C_sR_{ph}\times 10^6 = 10$, 3, 1, 0.3, and 0 (m) and scaled single scattering albedos due to the particles $\omega_{ps}=0$, 0.7, and 1, where

$$\omega_{ps} = (1-f)\,\omega_p/(1-\omega_p f) \tag{24a}$$

and

$$\omega_p = \sigma_p/(\sigma_p+\kappa_p) \tag{24b}$$

We also note that C_sR_{ph}/λ represents the spectral optical ra-

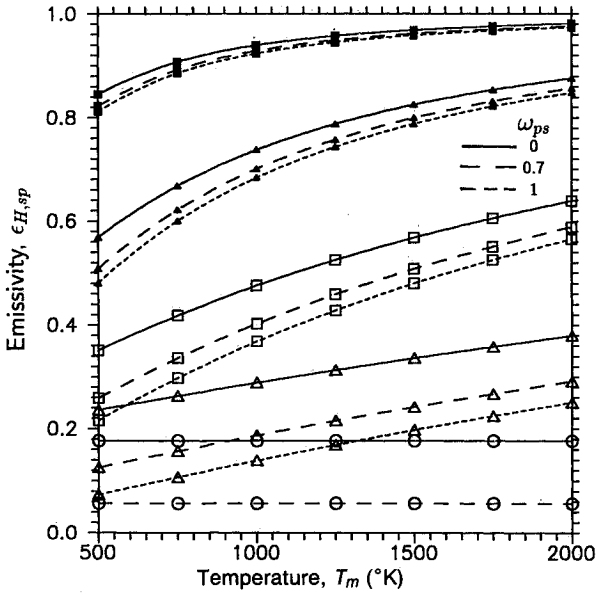

Fig. 2 Effect of scaled scattering albedo, soot volume fraction distance, and temperature on the total hemispherical emissivity for a mixture containing soot and particles; $(1-\omega_p f)\tau_p = 0.1$ and $C_sR_{ph}\times 10^6 =$ ■ 10, ▲ 3, □ 1, △ 0.3, ○ 0 (m).

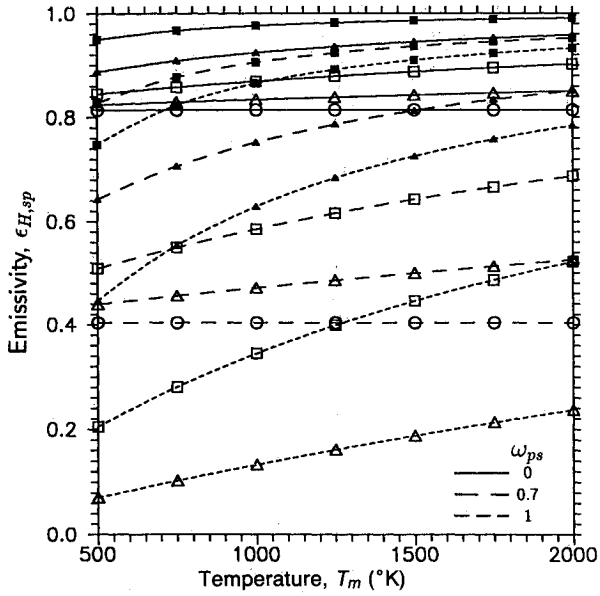

Fig. 4 Effect of scaled scattering albedo, soot volume fraction distance, and temperature on the total hemispherical emissivity for a mixture containing soot particles; $(1-\omega_p f)\tau_p = 1$ and $C_sR_{ph}\times 10^6 =$ ■ 10, ▲ 3, □ 1, △ 0.3, ○ 0 (m).

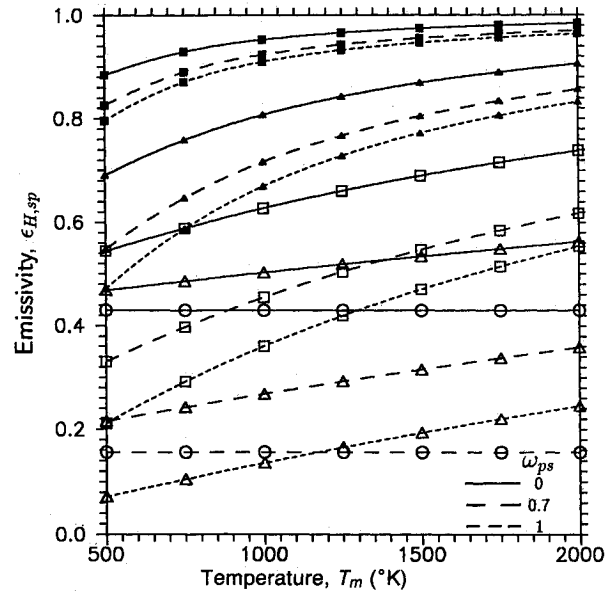

Fig. 3 Effect of scaled scattering albedo, soot volume fraction distance, and temperature on the total hemispherical emissivity for a mixture containing soot particles; $(1-\omega_p f)\tau_p = 0.3$ and $C_sR_{ph}\times 10^6 =$ ■ 10, ▲ 3, □ 1, △ 0.3, ○ 0 (m).

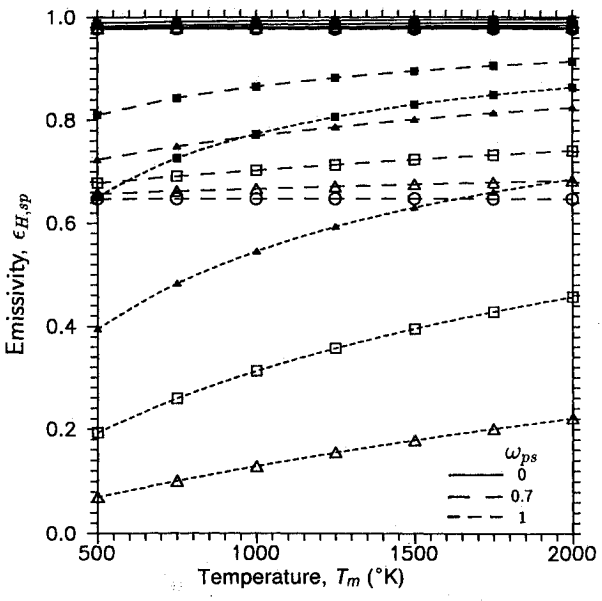

Fig. 5 Effect of scaled scattering albedo, soot volume fraction distance, and temperature on the total hemispherical emissivity for a mixture containing soot and particles; $(1-\omega_p f)\tau_p = 3$ and $C_sR_{ph}\times 10^6 =$ ■ 10, ▲ 3, □ 1, △ 0.3, ○ 0 (m).

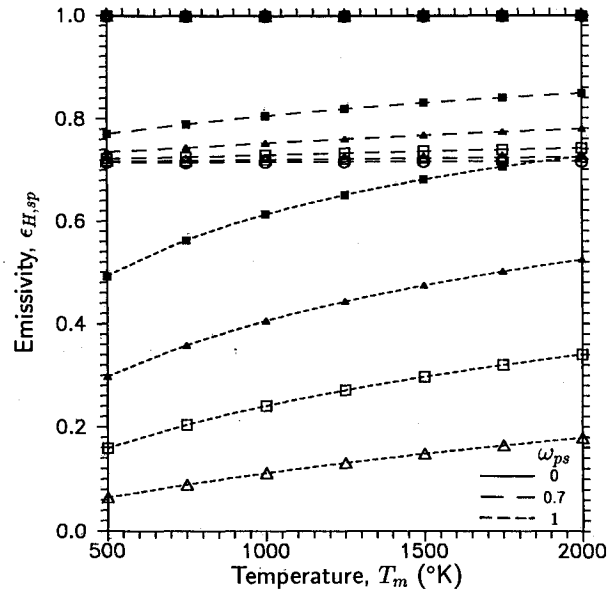

Fig. 6 Effect of scaled and scattering albedo, soot volume fraction distance, and temperature on the total hemispherical emissivity for a mixture containing soot and particles; $(1-\omega_p f)\tau_p = 10$ and $C_s R_{ph} \times 10^6 =$ ■ 10, ▲ 3, □ 1, △ 0.3, ○ 0 (m).

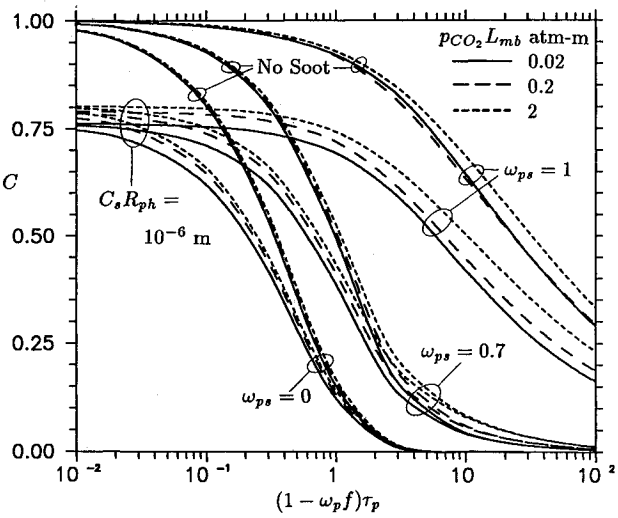

Fig. 7 Effects of scaled particle optical radius $(1-\omega_p f)\tau_p$ on the correction factor C for different scaled scattering albedos, soot volume fraction distances, and pressure path legends of CO_2 at a mixture temperature $T_m = 500$ K; $C_s R_{ph} = 0$, and 10^{-6} m.

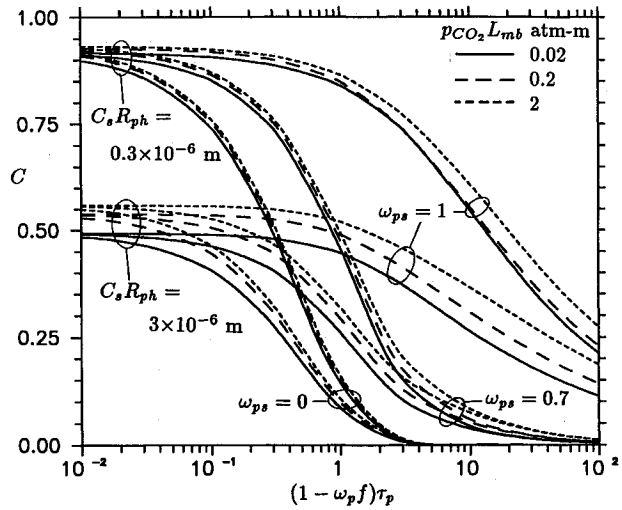

Fig. 8 Effects of scaled particle optical radius $(1-\omega_p f)\tau_p$ on the correction factor C for different scaled scattering albedos, soot volume fraction distances, and pressure path lengths of CO_2 at a mixture temperature $T_m = 500$ K; $C_s R_{ph} = 0.3\times10^{-6}$, and 3×10^{-6} m.

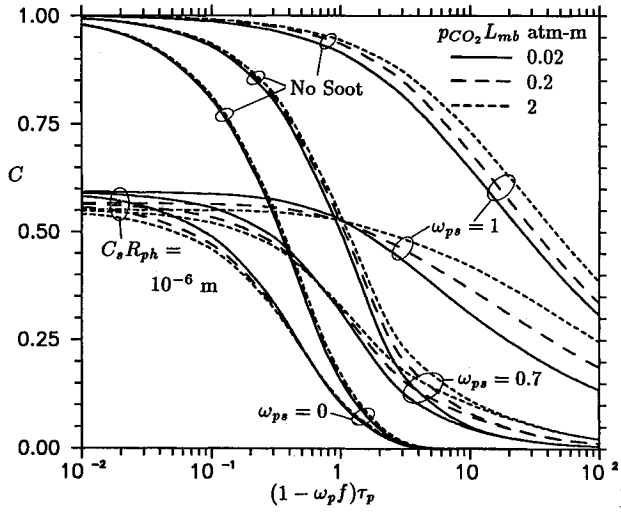

Fig. 9 Effects of scaled particle optical radius $(1-\omega_p f)\tau_p$ on the correction factor C for different scaled scattering albedos, soot volume fraction distances, and pressure path lengths of CO_2 at a mixture temperature $T_m = 2000$ K; $C_s R_{ph} = 0$, and 10^{-6} m.

dius due to the soot. As shown in Fig. 2 for the case of a small value of the particle optical radius, $(1-\omega_p f)\tau_p = 0.1$, where

$$\tau_p = (\sigma_p + \kappa_p) R_{ph} \tag{25}$$

the contribution from the soot to the emissivity is large for values of $C_s R_{ph} \geq 10^{-6}$ m. Further inspection of this figure reveals that even for such a small scaled optical radius that the particles effectively shield emission from the medium. For example, at a mixture temperature of 1250 K, the emissivity for a purely absorbing medium is reduced by about 20% if purely scattering particles are added to it so that $(1-\omega_p f)\tau_p = 0.1$. However, for smaller values of $C_s R_{ph} \leq 10^{-6}$ m, the emissivity is strongly affected by the value of the scaled single scattering albedo. This effect is more pronounced in Figs. 3–6, where the scaled optical radius is increased. Examination of these figures reveals that the emissivity does not approach unity, even in the optically thick cases. Here, optically thick implies that the scaled optical radius $(1-\omega_p f)\tau_p$ is much larger than unity. Such an effect is also demonstrated in Table 1. Consequently, scattering effects are important in the analysis of IR signatures from rocket plumes containing significant amounts of Al_2O_3 particles, which in a solid phase are nearly purely scattering, as noted by Nelson.[20,21] However, the loss of emission cross section upon solidification of molten aluminum oxide as well as the presence of impurities are important factors in the analysis of IR signatures.[22]

The enhancement factor C, or more appropriately, the correction factor is shown in Figs. 7 and 8 and Figs. 9 and 10 for a gas containing CO_2 at a mixture temperature $T_m = 500$ and 2000 K, respectively, and pressure path lengths $p_{CO_2} L_{mb} =$ 0.02, 0.2, and 2 atm-m, scaled single scattering albedos due to particles $\omega_{ps} = 0$, 0.7, and 1, and soot volume fraction distances $C_s R_{ph} \times 10^6 = 0$, 0.3, 1, and 3 m. These calculations are based on setting $b = 0.05$ in Eq. (18b), adjusting the exponential decay width $\bar{\omega}_i$ upward by 30%,[9] and assuming $p_{CO_2} \to 0$. Examination of these figures reveals several interesting aspects on the interaction among gases, soot, and particles. These effects are in particular related to the magnitude and the behavior of C in the limits of zero particle optical radius $[(1-\omega_p f)\tau_p \to 0]$ and in the limit of infinite particle optical radius $[(1-\omega_p f)\tau_p \to \infty]$. First, the correction factor never ex-

ceeds unity; it approaches unity only in such cases where the medium is optically thin and contains only purely scattering particles. Thus, this limiting value of C being close to unity is in agreement with investigation in plane-parallel geometry,[19] and no enhancement ($C > 1$) has been calculated of the gaseous emission for the considered pressure path lengths.

Second, we note in these figures that, for larger values of the optical radius, the correction factor in all cases approaches a very small value in an exponential-like manner. One should expect such behavior not only from physical grounds but also as a result of the first-order mathematical formulation. Thus one may suggest plotting the results on a log-log scale, but such plotting neither changes nor simplifies the interpretation of the results. The addition of significant amounts of soot does not change the exponential-like decaying behavior of the correction factor. Instead the presence of the soot reduces the range of values the correction factor can take, which implies a reduced transmissivity of the gaseous emission. For example, in the case of a soot volume fraction distance $C_sR_{ph} = 3 \times 10^{-6}$ m and a mixture temperature $T_m = 500$ K, the correction factor $0 \le C \le 0.56$ as shown in Fig. 8. Considering the same soot volume fraction distance, but an increase in the mixture temperature to $T_m = 2000$ K yields the bound $0 \le C \le 0.25$ in Fig. 10. Such result is expected since for larger mixture temperatures the characteristic wavelengths decrease leading to increased spectral absorption coefficients and spectral optical radii of the soot. Hence, the correction factor is not only strongly dependent on the soot volume fraction distance but also strongly dependent on the mixture temperature.

Third, these figures also reveal several clearly noticeable trends in the limit of no particles $[(1-\omega_p f)\tau_p \to 0]$ and in the limit of an infinite scaled particle optical radius $[(1-\omega_p f)\tau_p \to \infty]$. For example, there results a leveling of the curves for the smaller values of the particle optical depth indicating a weak dependence of C on the scaled optical radius. That is, the transmissivity of the particulate phase to gaseous emission is primarily due to the soot volume fraction distance. For larger values of the scaled optical depth, however, the results for the correction factor approaches that for no soot within the medium; this result is expected since a much larger contribution to the extinction coefficient comes from the particles. The shielding of gaseous emission is thus due to the optical depth and radiative properties of the particles. Hence, for a specified pressure path length, the curves covering the smaller values of the scaled optical radius coalesce into a single curve for a given pressure path length and for larger values of the scaled optical radius, the results coalesce into single curve for a given value of the scaled single scattering albedo.

Fourth, a slightly rising then a monotonically decaying value of C is observed in Fig. 10 for $C_sR_{ph} = 3 \times 10^{-6}$ m and $\omega_{ps} = 1$. This effect may be interpreted as a small increase in the particulate transmittance to the gaseous emission as the scaled optical radius increases. Physically, the slight rising and then the decaying value of C is attributed to a geometrical effect similar to the one observed in plane-parallel media.[19] That is, radiation emitted near large values of the slant path (θ near 0 deg) may be scattered into directions with short slant paths (θ near 90 deg and ϕ near 0 deg).

In Figs. 11 and 12, the correction factor C for H_2O for a mixture temperature of 500 K, the pressure path lengths $p_{H_2O}L_{mb} = 0.02$, 0.2, and 2 atm-m, scaled single scattering albedos due to particles $\omega_{ps} = 0$, 0.7 and 1, and soot volume fraction distances $C_sR_{ph} \times 10^6 = 0$, 0.3, 1, and 3 m. These calculations are based on setting $b = 0.05$ in Eq. (18b), adjusting the exponential decay width $\bar{\omega}_i$ upward by 30%,[9] and assuming $p_{H_2O} \to 0$. Comparison of these two figures with Figs. 7 and 8, respectively, reveals that the correction factor is quite insensitive to whether one considers CO_2 or H_2O as the participating gas, which may be extended to consideration of mixtures of these gases of the same pressure path length and temperature.

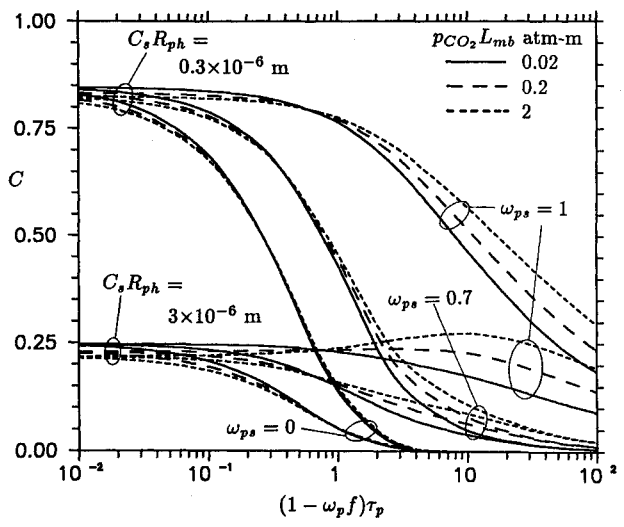

Fig. 10 Effects of scaled particle optical radius $(1-\omega_p f)\tau_p$ on the correction factor C for different scaled scattering albedos, soot volume fraction distances, and pressure path lengths of CO_2 at a mixture temperature $T_m = 2000$ K; $C_sR_{ph} = 0.3 \times 10^{-6}$, and 3×10^{-6} m.

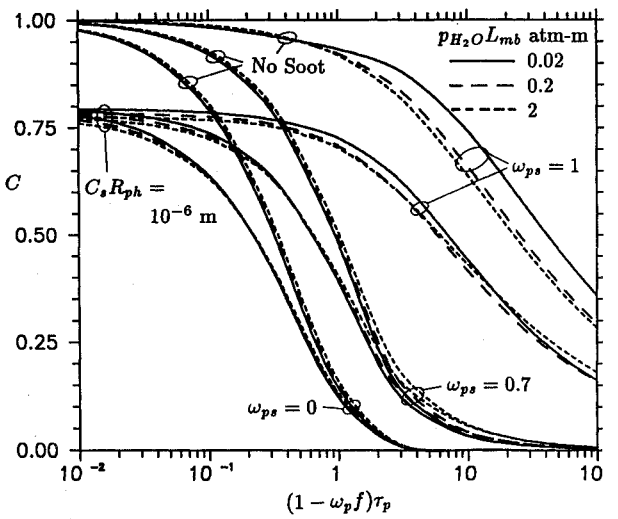

Fig. 11 Effects of scaled particle optical radius $(1-\omega_p f)\tau_p$ on the correction factor C for different scaled scattering albedos, soot volume fraction distances, and pressure path lengths of H_2O at a mixture temperature $T_m = 500$ K; $C_sR_{ph} = 0$, and 10^{-6} m.

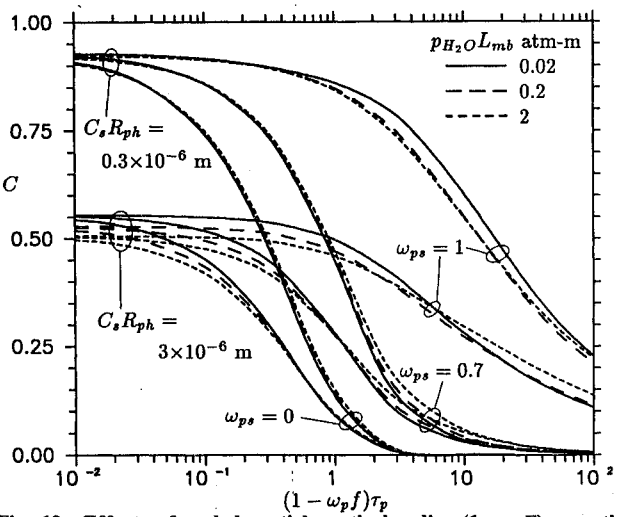

Fig. 12 Effects of scaled particle optical radius $(1-\omega_p F)\tau_p$ on the correction factor C for different scaled scattering albedos, soot volume fraction distances, and pressure path lengths of H_2O at a mixture temperature $T_m = 500$ K; $C_sR_{ph} = 0.3 \times 10^{-6}$, and 3×10^{-6} m.

Thus the discussion on the physical significance of the correction factor discussed previously also is applicable for the case of water vapor. With such similar behavior, results for a mixture temperature of 2000 K are not presented.

Conclusions

A method for estimating the total hemispherical emissivity for an isothermal absorbing, emitting, anisotropically scattering cylinder has been presented. Based on the presented results, the following conclusions have been reached:

1) The calculational method yields results that are physically realistic for all considered cases of optical dimensions and single scattering albedos.

2) The use of a two-point quadrature for performing the spectral integration over each molecular gas band produces total gas emissivities that are in excellent agreement with other methods as well as experimental results.

3) The correction factor C never exceeds unity, which indicates that the total hemispherical emissivity is not enhanced by the type of particles considered in the present study.

4) The correction factor C is quite insensitive to whether CO_2 or H_2O gases are considered. Thus one may expect that similar results would be obtained if a mixture of these gases are analyzed, thereby extending the range of the charts for the correction factor.

Appendix: Treatment of Band Overlapping

The treatment of band overlapping is rather cumbersome and introduces a considerable complexity into the analysis. Such effects are considered in the present analysis in a similar manner, except for one case, as described by Edwards,[9] and the details of his treatment are not discussed in this work. The exception to his is the treatment of the overlapping between the rotational and 6.3-μm bands of H_2O. Actually, overlapping between the rotational and 6.3-μm bands of water vapor is treated differently than both Edwards[9] and Edwards and Balakrishnan.[23] First, the new band parameters of Modak[17] are used. Second, emission from wavenumbers below 140 cm^{-1} is neglected, which implies that the rotational band is an asymmetric one. Third, it is assumed that the overlapping interaction between these two bands is *negligible*, that is, the transmissivity is very nearly the product of the transmissivities of each band. In view of these assumptions, the spectral absorption coefficient is additive within the overlapping interval and is equal to the sum of the rotational and the 6.3-μm spectral absorption coefficients determined separately, as illustrated in Fig. A1. The use of the two-point quadrature over the overlapping rotational and 6.3-μm bands requires a modification of the procedure described in the section on wavelength integration. The wavenumber at which the spectral absorption coefficients of the rotational and 6.3-μm bands are equal is determined from Eq. (6) by setting

$$\kappa_{g\nu_{rot}} = \kappa_{g\nu_{6.3}} \tag{A1}$$

Solving Eq. (A1) iteratively by Newton's method yields the new upper band limit for the rotational band and the new lower limit for the 6.3-μm band. The upper limit of the 6.3-μm band is determined from Eq. (17). The quadrature points are now determined as

$$\text{Rotational band:} \begin{cases} \nu_{1,1} = \nu_{\text{rot},1} = \nu_{c,\text{rot}} + 0.2113\Delta\nu_{\text{rot}} \\ \nu_{1,2} = \nu_{\text{rot},2} = \nu_{c,\text{rot}} + 0.7887\Delta\nu_{\text{rot}} \\ \Delta\nu_1 = \Delta\nu_{\text{rot}} \end{cases} \tag{A2}$$

$$\text{6.3-}\mu\text{m Lower band:} \begin{cases} \nu_{2,1} = \nu_{6.3,1} = \nu_{c,6.3} - 0.2113\Delta\nu_{l,6.3} \\ \nu_{2,2} = \nu_{6.3,2} = \nu_{c,6.3} - 0.7887\Delta\nu_{l,6.3} \\ \Delta\nu_2 = \Delta\nu_{l,6.3} \end{cases} \tag{A3}$$

$$\text{6.3-}\mu\text{m Upper band:} \begin{cases} \nu_{3,1} = \nu_{6.3,1} = \nu_{c,6.3} + 0.2113\Delta\nu_{u,6.3} \\ \nu_{3,2} = \nu_{6.3,2} = \nu_{c,6.3} + 0.7887\Delta\nu_{u,6.3} \\ \Delta\nu_3 = \Delta\nu_{u,6.3} \end{cases} \tag{A4}$$

It should be noted that, despite the effects of overlapping, Eq. (20) still is applicable for the integration over all wavenumbers, but the blackbody function should not be determined at the band center of the rotational band; instead the blackbody function should be determined at the two wavenumbers corresponding to the quadrature points. To use Eq. (20), however, it is necessary to include the above three bands and the 2.7-, 1.87-, and 1.38-μm bands as well, i.e., the value of N has been changed from 5 to 6 for H_2O.

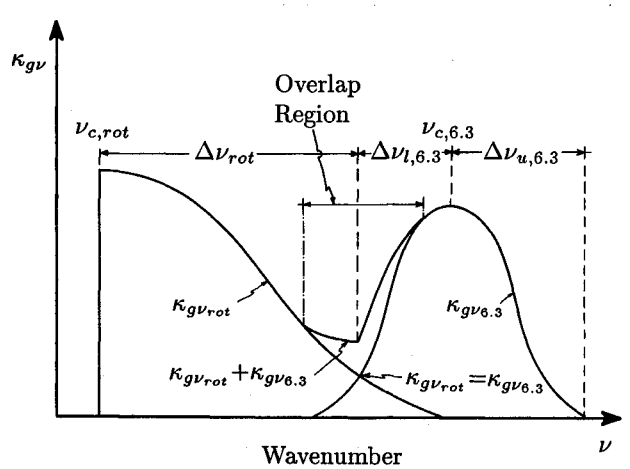

Fig. A1 Description of treatment of overlapping of the rotational and the 6.3 μm vibration-rotation bands of water vapor. The absorption coefficient is assumed additive in the overlap region.

Acknowledgment

The partial support received from the Office of Naval Research, Grant N00014-86-K-0468, is gratefully acknowledged.

References

[1]Felske, J. D., and Lee, K. M., "Nongray Particulate Radiation in an Isothermal Cylindrical Medium," *Journal of Heat Transfer,* Vol. 103, Feb. 1981, pp. 121-126.

[2]Tabanfar, S., and Modest, M. F., "Radiative Heat Transfer in a Cylindrical Mixture of Nongray Particulates and Molecular Gases," *Journal of Quantitative Spectroscopy and Radiative Transfer,* Vol. 30, No. 6, 1983, pp. 555-570.

[3]Azad, F. H., and Modest, M. F., "Evaluation of the Radiative Heat Flux in Absorbing, Emitting and Linear-Anisotropically Scattering Cylindrical Media," *Journal of Heat Transfer,* Vol. 103, May 1981, pp. 350-356.

[4]Der, J. J., and Nelson, D. A., "Internal Radiative Heating from Aluminum Oxide Particles in Solid Propellant Rocket Motors," AIAA 85-1397, July 1985.

[5]Buckius, R. O., and Fernandez-Fraga, A., "The Optical Path Length Approach to Radiation Heat Transfer with Isotropic Scattering and Gaseous Absorption," *Journal of Quantitative Spectroscopy and Radiative Transfer,* Vol. 24, No. 1, 1980, pp. 1-13.

[6]Buckius, R. O., "The Effect of Molecular Gas Absorption on Radiative Heat Transfer with Scattering," *Journal of Heat Transfer,* Vol. 104, Nov. 1982, pp. 580-586.

[7]Skocypec, R. D., and Buckius, R. O., "Total Hemispherical Emittances for CO_2 or H_2O Including Particulate Scattering," *International Journal of Heat and Mass Transfer,* Vol. 27, No. 1, 1984, pp. 1-13.

[8]Özişik, M. N., *Radiative Transfer,* Wiley, New York, 1973, p. 264.

[9]Edwards, D. K., "Molecular Gas Band Radiation," *Advances in Heat Transfer,* Vol. 12, edited by T. F. Irvine, Jr. and J. P. Hartnett, Academic, New York, 1976, pp. 115-193.

[10]Edwards, D. K., and Balakrishnan, A., "Slab Band Absorptance for Molecular Gas Radiation," *Journal of Quantitative Spectroscopy and Radiative Transfer,* Vol. 12, 1972, pp. 1379-1387.

[11]Siegel, R., and Howell, J. R., *Thermal Radiation Heat Transfer,* 2nd ed., McGraw-Hill, New York, 1981.

[12]Potter, J. F., "The Delta Function Approximation in Radiative Transfer Theory," *Journal of the Atmospheric Sciences,* Vol. 27, Sept. 1970, pp. 943–949.

[13]Kofink, W., "Complete Spherical Harmonics Solution of the Boltzmann Equation for Neutron Transport in Homogeneous Media with Cylindrical Geometry," *Nuclear Science and Engineering,* Vol. 6, 1959, pp. 475–486.

[14]Thynell, S. T., and Özişik, M. N., "Integral Form of Equation of Transfer for an Isotropically Scattering, Inhomogeneous Solid Cylinder," *Journal of Quantitative Spectroscopy and Radiative Transfer,* Vol. 36, No. 6, 1986, pp. 497–503.

[15]Thynell, S. T., and Özişik, M. N., "Radiation Transfer in Absorbing, Emitting, Isotropically Scattering, Homogeneous Cylindrical Media," *Journal of Quantitative Spectroscopy and Radiative Transfer,* Vol. 38, No. 6, 1987, pp. 413–426.

[16]Hottel, H. C., "Radiant Heat Transmission," *Heat Transmission,* 3rd ed., edited by W. H. McAdams, McGraw-Hill, New York, 1954, Chap. 4.

[17]Modak, A. T., "Exponential Wide Band Parameters for the Pure Rotational Band of Water Vapor," *Journal of Quantitative Spectroscopy and Radiative Transfer,* Vol. 21, 1979, pp. 131–142.

[18]Ludwig, C. B., Malkmus, W., Reardon, J. E., and Thomson, J. A. L., *Handbook of Infrared Radiation from Combustion Gases,* edited by R. Goulard and J. A. L. Thomson, NASA SP-3080, 1973.

[19]Goodwin, D. G., and Ebert, J. L., "Rigorous Bounds on the Radiative Interaction Between Real Gases and Scattering Particles," *Journal of Quantitative Spectroscopy and Radiative Transfer,* Vol. 37, No. 5, pp. 501–508.

[20]Nelson, H. F., "Influences of Particulates on Infrared Emission from Tactical Rocket Exhausts," *Journal of Spacecraft and Rockets,* Vol. 21, No. 5, 1984, pp. 425–432.

[21]Nelson, H. F., "Influence of Scattering on Infrared Signatures of Rocket Plumes," *Journal of Spacecraft and Rockets,* Vol. 21, No. 5, 1984, pp. 508–510.

[22]Edwards, D. K., and Bobco, R. P., "Effect of Particle Size Distribution on the Radiosity of Solid-Propellant Rocket Motor Plumes," *Spacecraft Radiative Transfer and Temperature Control,* Progress in Astronautics and Aeronautics, Vol. 83, edited by T. E. Horton, AIAA, New York, 1982, pp. 169–188.

[23]Edwards, D. K., and Balakrishnan, A., "Thermal Radiation by Combustion Gases," *International Journal of Heat and Mass Transfer,* Vol. 16, No. 1, 1973, pp. 25–40.